Journal of Cluster Science (2026) 37:140
https://doi.org/10.1007/s10876-026-03099-8

ORIGINAL PAPER

Structural evolution and combustion energy of Al-B clusters

Elizaveta E. Vaneeva[1,2] · Anastasiia A. Mikhailova[1,2] · Sergey V. Lepeshkin[1,2] · Alexey P. Maltsev[1] · Artem R. Oganov[1,3]

Received: 6 April 2026 / Accepted: 17 August 2026
© The Author(s), under exclusive licence to Springer Science+Business Media, LLC, part of Springer Nature 2026

Abstract
Systematic structure prediction of Al_nB_m clusters ($0 \le n, m \le 16$) was performed to explore their structural diversity, stability, and combustion-related properties. The predicted low-energy structures exhibit distinct structural motifs determined by the topology of the boron subnetwork, ranging from isolated boron atoms embedded in aluminum frameworks to dense and perforated boron networks with increasing boron content. The stability of Al_nB_m clusters was analyzed using criteria adopted in nanocluster studies. In particular, the predicted enhanced stability of Al_{13} and $Al_{12}B$ is consistent with available experimental mass-spectrometric data. Fragmentation analysis indicates that mixed Al_nB_m clusters typically dissociate through the loss of a single aluminum atom. At the nanoscale, pure boron and boron-rich Al_nB_m clusters exhibit higher Gibbs free energies and specific energy of combustion than aluminum clusters, in contrast to bulk behavior. Smaller clusters exhibit larger energy output because of their higher fraction of reactive surface atoms, and this size dependency becomes less pronounced for aluminum-richer compositions.

Introduction

The development of high-energy-density fuels is a key challenge for next-generation propulsion and power systems. One promising approach is the incorporation of metal or metalloid nanoclusters into conventional liquid hydrocarbon fuels [1]. Due to their small size, nanoclusters possess a large fraction of surface atoms, which makes them highly reactive and allows for faster and more complete oxidation during combustion. This often results in increased heat release, shorter ignition delay, and faster flame propagation [2]. Among the various candidates, it is aluminum and boron that are the most widely explored. Their relatively low ignition temperatures, high heats of combustion, and compatibility with liquid-fuel formulations make them especially effective in improving the performance of traditional hydrocarbon fuels [3]. Both elements belong to group 13 and are isoelectronic, having three valence electrons, yet they exhibit different bonding characteristics and physical behavior. Aluminum has relatively diffuse valence orbitals, which give rise to delocalized, weakly directional metallic bonding, hence, it has a relatively low surface energy: breaking metallic bonds and forming surfaces is energetically inexpensive, and dangling bonds are not strongly penalized. Boron, in contrast, forms strongly directional, 2-center and multicenter covalent bonds and behaves as a frustrated semiconductor. In such systems, dangling bonds are energetically costly, leading to high surface energies and pronounced surface reconstruction.

These electronic differences govern the structural chemistry of aluminum and boron and are directly reflected in their preferred cluster geometries. Small aluminum clusters favor compact, highly symmetric structures, most notably the icosahedral Al_{13} "magic" cluster, and icosahedral motifs are also common in aluminum-based quasicrystals. In contrast, crystalline boron consists of hollow B_{12} icosahedra arranged in complex networks, yet such units are absent in small free boron clusters, which instead adopt planar or quasi-planar structures over a wide size range [4]. Another important distinction lies in bond strengths. A single B-B bond (3.08 eV) [5] is significantly stronger than a single Al-Al bond (1.37 eV) [5] due to its covalent nature.

✉ Elizaveta E. Vaneeva
Elizaveta.Vaneeva@skoltech.ru

1 Skolkovo Institute of Science and Technology, Bolshoy Boulevard 30, bld. 1, Moscow 121205, Russian Federation

2 Lebedev Physical Institute, Russian Academy of Sciences, Leninsky Ave. 53, Moscow 119991, Russian Federation

3 Sber University, Universitetskaya Street 11, Anosino, Istra urban district, Moscow Region 143581, Russian Federation

Published online: 27 August 2026

From an energetic perspective, boron has long been considered as one of the most promising energetic additives for hydrocarbon fuels due to its exceptionally high gravimetric (≈58 MJ/kg) and volumetric (≈131 MJ/L) combustion energy densities [3]. Its combustion releases large amounts of heat and can significantly increase the flame temperature, thereby improving the thermal efficiency and thrust of propulsion systems. However, the practical utilization of boron remains challenging. Although boron has a higher energy density than aluminum, its practical use is hindered by the rapid formation of a dense, B_2O_3 layer that blocks oxygen diffusion to the boron core, leading to incomplete combustion and the generation of solid oxide particles that ultimately reduce performance and can cause nozzle clogging [6, 7]. As a result, boron suffers from long ignition delays, incomplete oxidation, and reduced overall energy release [8]. These limitations hinder its direct use in propulsion systems despite its outstanding theoretical energy content.

Aluminum, in contrast, ignites at lower temperature and exhibits faster oxidation kinetics under combustion conditions than boron, which together with its high heat of combustion (~31 MJ/kg) makes it an effective additive and ignition promoter in propellants and explosives [9]. When aluminum and boron are combined, the rapid ignition of aluminum can slow down the growth of the surface B_2O_3 layer and partially disrupt the existing oxide film. As a result, oxygen gains easier access to the boron, enabling more complete oxidation and, consequently, more complete boron combustion [5]. Such mixed clusters or composite additives retain high theoretical energy density of boron while benefiting from superior ignition and oxidation characteristics of aluminum, making Al-B materials attractive candidates for next-generation high-energy fuels.

However, clusters of mixed compositions (Al_nB_m) have not been investigated properly until now. The experimental study of these clusters is a difficult task, therefore, it is advisable to start by identifying the most promising of them at the fundamental level. Only a few studies analyzed the structure and properties of certain neutral Al_nB_m clusters of special composition: Al_nB_m ($n+m \leq 7$) [10] and AlB_n ($n=0-20$) [11, 12]. Thus, most existing studies are limited to examining only a small number of fixed compositions, whereas multicomponent clusters, which are of greater interest for practical applications, may have unexpected stoichiometries very different from those of solid phases.

In this work, we conduct a systematic study of Al_nB_m nanoclusters in a wide compositional range ($0 \leq n \leq 16$, $0 \leq m \leq 16$). We utilize global optimization methods in conjunction with density functional theory (DFT) calculations to determine ground-state structures. We also investigate the reactive (energetic) characteristics of Al–B clusters, including combustion energy that indicates their potential energy release upon oxidation, and identify the most stable ("magic") compositions to elucidate the structure–stability relationships.

Computational methods

The structures of Al_nB_m clusters were determined using an evolutionary variable-composition global optimization algorithm implemented in the USPEX code [9, 10]. To ensure efficient and reliable structure prediction, the computational procedure consisted of several steps. First, the USPEX search was performed using an evolutionary algorithm in combination with the ab initio VASP code [13, 14], which employs the projector-augmented wave method [15] and the Perdew-Burke-Ernzerhof (PBE) exchange-correlation functional [16], taking spin polarization into account. Global optimization requires a very large number of structural relaxations across the full Al_nB_m compositional space, hence, the PBE functional with PAW potentials was selected at the search stage because of its robustness and computational efficiency in screening a large number of candidate structures. Subsequently, the 10 lowest-energy isomers from each composition were selected for further refinement using the GAUSSIAN software, applying the B3LYP hybrid functional and the 6-311G+(d, p) basis set, using spin multiplicity corresponding to the lowest energy state [17]. This level of theory is more appropriate for the final structural and energetic analysis of finite molecular clusters. We calculated the vibrational frequencies in all obtained structures and verified that each possesses 3N-6 positive frequencies. For each ground state structure we calculated Gibbs free energy at T = 300 K, computing partition functions related to vibrations, translations, rotations, and electronic configurations.

Regarding the stability of Al_nB_m molecules, we use the same criteria as previously used [18–25], based on their ground-state energies $E(n, m)$. In the first criterion, we consider stability of a cluster with respect to the nearest compositions obtained by adding or removing one Al or one B atom. The corresponding measures of stability are written as follows:

$$\Delta^2_{\mathrm{Al}} E(n,m) = E(n+1,m) + E(n-1,m) - 2E(n,m) \quad (1a)$$

$$\Delta^2_{B} E(n,m) = E(n,m+1) + E(n,m-1) - 2E(n,m) \quad (1b)$$

Then, we characterize the degree of stability of the molecule by the minimum of these values: $\Delta^2{}_{\mathrm{min}} = \min\{\Delta^2{}_{\mathrm{Al}}E, \Delta^2{}_{\mathrm{B}}E\}$. Molecules with a positive $\Delta^2{}_{\mathrm{min}}$ are referred to as "magic", drawing an analogy to "magic" clusters in nanoscience and "magic" nuclei in nuclear physics. It is observed that

"magic" nanoclusters are more abundant than others, which was confirmed in a number of studies [4, 18–23, 25].

Another criterion is stability with respect to fragmentation. To this end, we consider all possible channels of fragmentation of a given molecule for the decomposition into two fragments:

$$\mathrm{Al}_n\mathrm{B}_m \rightarrow \mathrm{Al}_a\mathrm{B}_b + \mathrm{Al}_{n-a}\mathrm{B}_{m-b}, \text{where } 0 \le a \le m, 0 \le b \le n \quad (2)$$

The fragmentation energy of each reaction is found as:

$$E_{frag,2}(n,m,a,b) = E(a,b) + E(n-a,m-b) - E(n,m) \quad (3)$$

We are looking for the decomposition into the most stable fragments, hence, we calculated the minimal value of all fragmentation energies (and if it is negative, the cluster will be unstable with respect to fragmentation):

$$E_{frag,2}(n,m) = min_{a,b}E_{frag,2}(n,m,a,b) \quad (4)$$

We additionally analyze the energetics of elementary composition-changing processes involving the addition or removal of a single atom. The corresponding energies were calculated as:

$$\Delta E_{add/rem}(n,m) = min({E_{add}}^{Al}(n,m), {E_{add}}^{B}(n,m)) - min({E_{rem}}^{Al}(n,m), {E_{rem}}^{B}(n,m)) \quad (5)$$

where

$${E_{add}}^{Al}(n,m) = E(n+1,m) - E(n,m) - E(1,0) \quad (6)$$

$${E_{add}}^{B}(n,m) = E(n,m+1) - E(0,1) - E(n,m) \quad (7)$$

$${E_{rem}}^{Al}(n,m) = E(n-1,m) + E(1,0) - E(n,m) \quad (8)$$

$${E_{rem}}^{B}(n,m) = E(n,m-1) + E(0,1) - E(n,m) \quad (9)$$

Results and discussion

Structure and stability of nanoclusters

We explored the ground-state structures of Al_nB_m clusters within a broad compositional range of $0 \le n, m \le 16$. The *xyz* coordinates of all optimized ground-state structures are provided in ESI Section S2.

Pure clusters of aluminum [26, 27] and boron [28–30] were studied in detail before, also by our group [4]. In addition, mixed metal-boron clusters have attracted considerable attention because incorporation of metal atoms can substantially modify the structural motifs, stability of boron frameworks [31–36]. However, compared with other metal-boron systems, aluminum-boron clusters have been explored only for relatively small sizes and/or restricted compositions: AlB_m (m=0–20) [11, 12], Al_nB_m ($n+m \le 7$) [10, 37]. For the compositions overlapping with previous works, the symmetries and structural motifs obtained in the present study are generally consistent with the reported ground-state structures. A detailed comparison of cluster symmetries with previous studies is provided in ESI Table S1. All structures agree with the literature data except for one case - Al_3B_3. For this composition, the symmetry of our ground-state structure differs from that reported previously; however, we identified a higher-energy isomer with the same symmetry as the literature structure, lying 0.215 eV above our ground state. The ground-state structures of numerous Al_nB_m (up to $0 \le n, m \le 16$) clusters were found for the first time. The ground-state structures of Al_nB_m nanoclusters can be classified into several distinct classes based on the structural characteristics of the boron fragments within each cluster (Fig. 1). Al-rich Al_nB_m nanoclusters ($m \le 4$ and $n+m \ge 7$) form *1st class* (Fig. 1a). The clusters have a nonplanar structure: an aluminum framework with a small isolated boron fragment inside. As the boron content increases, boron replaces aluminum, starting from the inner sites and moving outward, while the atomic arrangement remains fixed.

The *second class* of Al_nB_m (Fig. 1b) nanoclusters is defined by dense boron fragments that form well-organized nets. Unlike Al-rich clusters, the boron atoms interact closely, forming continuous or semi-continuous networks that resemble fragments of larger boron sheets. Depending on the aluminum environment, the boron fragments are planar, quasi-planar (exhibit a nearly planar geometry with slight deviations). There are exceptions with non-planar boron motifs with $5 \le m \le 7$. Notably, these boron networks correspond to the ground states of pure boron clusters [4]. Planar and quasi-planar nets are forming hexagonal or distorted hexagonal patterns, akin to borophene-like structures [38]. Structures along the diagonal $n+m$=22 exhibit pronounced layered motifs, reminiscent of those found in bulk aluminum boride AlB_2. However, unlike the planar boron layers observed in the bulk phases, the boron-rich fragments in these clusters adopt curved, nonplanar geometries.

As the boron concentration increases, aluminum atoms become embedded within the dense boron networks, displacing boron fragments and causing deviations from ideal compact structures (dense networks). Here gaps and irregularities appear, as if the once-unbroken sheet has been stretched and torn apart in places. This leads to the formation of a distinct class (*class 3*, Fig. 1c) of Al_nB_m clusters we call perforated networks. It is worth noting that chain-like

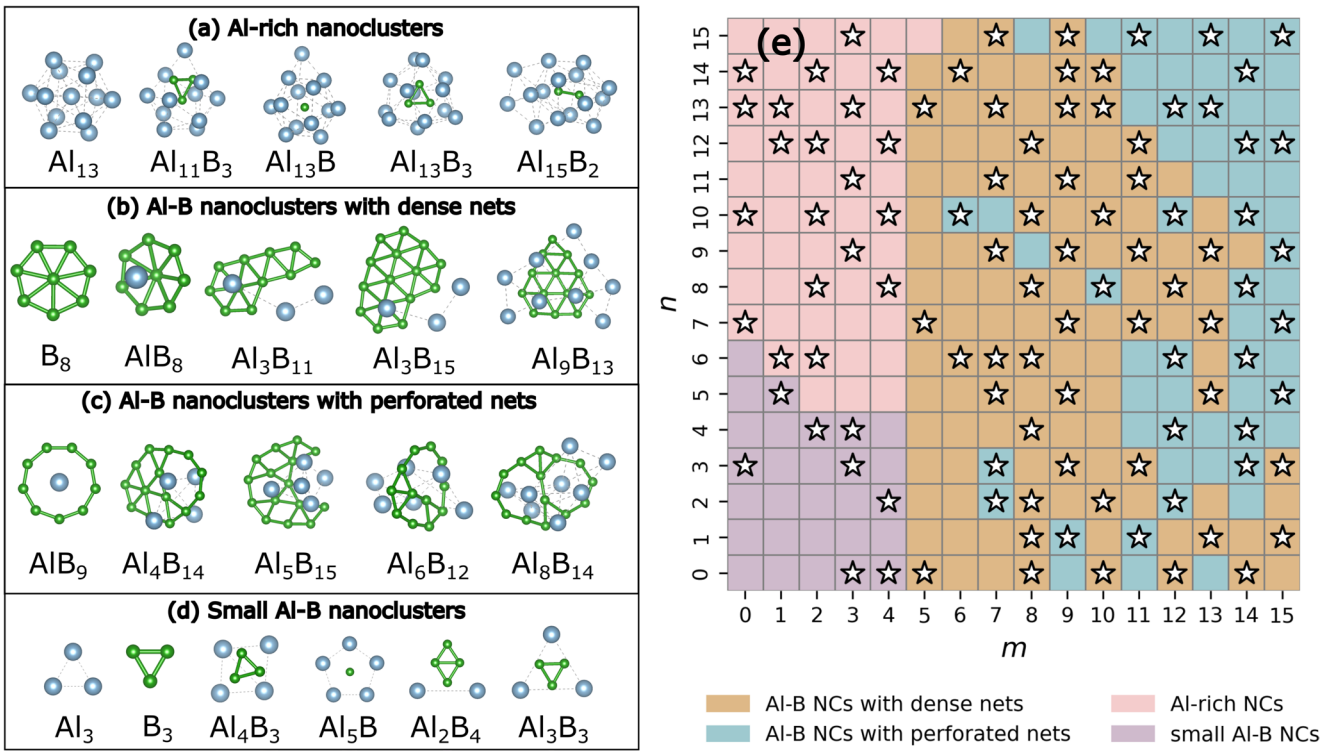

Fig. 1 Classification of Al_nB_m clusters into four categories based on their structural topology, illustrated using representative examples with $\Delta^2_{min}>0$: (**a**) Al-rich nanoclusters, (b) nanoclusters with dense networks, (**c**) nanoclusters with perforated networks, and (**d**) small Al–B nanoclusters. Blue and green spheres represent aluminum and boron atoms, respectively. (**e**) Schematic classification of Al_nB_m nanoclusters, where the composition space is divided into four regions according to structural characteristics. Stars indicate "magic" stoichiometries

structures formed by boron in structures with $n+m \geq 24$ are generally energetically unfavorable — previous studies consistently show boron's tendency to form tubular, cage-like and core-shell configurations. These perforated networks can be considered as transition states from dense nets to tubular or cage-like boron structures, such as B_{19} (D_{2d}) or the highly symmetric B_{20} (D_{10d}) [4]. However, in this case, the incorporation of aluminum appears to stabilize such unconventional boron fragments by providing a metallic framework that supports the existence of perforated networks. Such structural modifications significantly impact the local stability of the clusters.

Most of the small Al_nB_m clusters ($n+m \leq 6$ and $m \leq 4$) are categorized as *class 4*, (Fig. 1d) they adopt a planar arrangement, with the exception of Al_2B_2 and Al_3B_4, where boron atoms are repelled by aluminum, leading to a distorted geometry.

The stability of binary nanoclusters, characterized by Δ^2_{min} and E_{frag}, can be effectively visualized using 2D heatmaps (Fig. 2). In Fig. 2a, red regions indicate highly stable magic clusters, while blue areas represent unstable compositions where $\Delta^2_{min}<0$. Light blue regions correspond to unstable molecules, where $-0.4\ eV \leq \Delta^2_{min} \leq 0$.

An initial examination of the stability maps reveals distinct diagonal stability trends at $n+m$ = 6, 12, 16, 18, 20, and 22, particularly visible in the Δ^2_{min} map. Clusters along these diagonals exhibit closed-shell electronic structures and are predominantly associated with dense boron nets. For instance, clusters on the $n+m$ = 6 diagonal transition from pure 3D-shaped Al_6 to planar B_6, where boron atoms gradually replace aluminum, ultimately forming a separate boron sheet. Analogously, along the $n+m$ = 12, 16, and 18 diagonals, clusters evolve from pure aluminum to Al-rich compositions, then to structures with dense boron nets, and finally to pure boron clusters. In contrast, clusters along the $n+m$ = 20 and 22 diagonals are mainly composed of dense boron nets, which progressively transition into perforated boron structures. The upper right triangle of the Δ^2_{min} map (where $n+m \geq 24$), which primarily includes Al_nB_m clusters with perforated boron nets, displays a negative Δ^2_{min} value. This is due to the chain-like arrangement of boron in these structures, a configuration not typically associated with stable boron frameworks. However, when the aluminum content decreases to four or five atoms, some perforated nets transition to a planar geometry, thereby gaining local stability. Notably, several clusters exhibit "magic" stability despite having an odd number of electrons, which is often associated with high structural symmetry, as in B_3 (D_{3h}), B_5 (C_{2v}), AlB_8 (C_{7v}), Al_2B_7 (D_{7h}), Al_3 (D_{3h}), $Al_{12}B$ (D_{5d}), Al_{13} (I_h) and $Al_{14}B_9$ (C_2) (Fig. S2, ESI). However, magic behavior is not

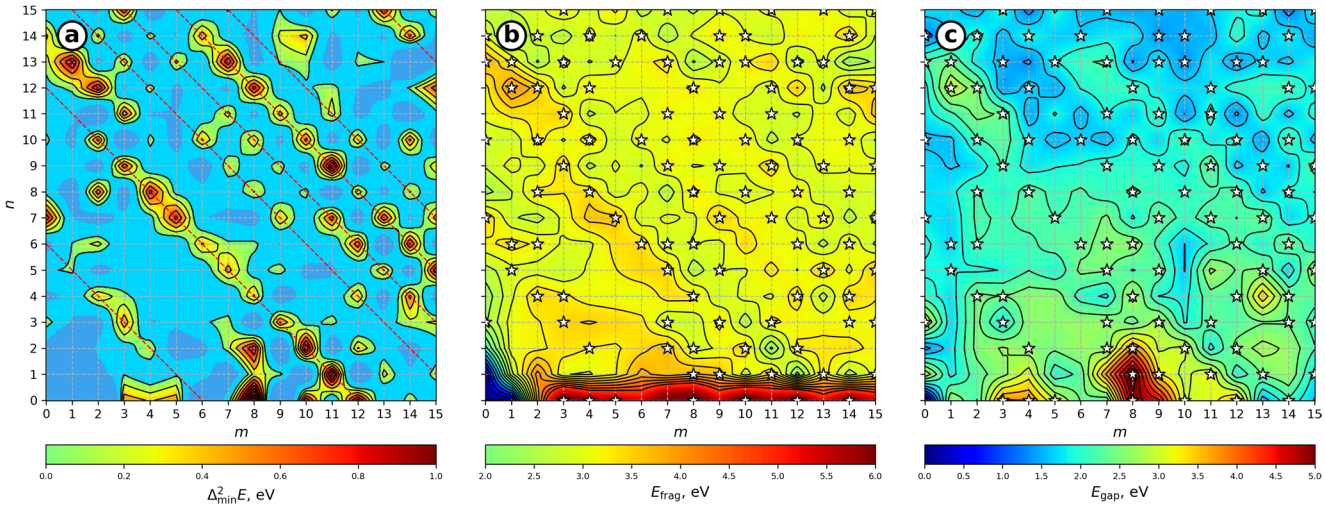

Fig. 2 Interpolated heatmaps of (**a**) Δ^2_{min} and (**b**) E_{frag} (c) HOMO-LUMO gap (in eV) for Al_nB_m nanoclusters as functions of n and m. Regions of structural instability are highlighted in blue. The dashed reference lines indicate "magic" nanoclusters located along the diagonals $n+m = 6$, 12, 16, 18, 20, and 22

exclusively symmetry-driven, since several clusters without symmetry also display enhanced stability, including Al_3B_{14} (C_1), $Al_{12}B_{11}$ (C_1), $Al_{13}B_{10}$ (C_1), and $Al_{13}B_{12}$ (C_1).

Al_{13} is a well-known magic aluminum cluster due to its highly symmetric Ih icosahedral structure and closed-shell character. Its enhanced stability and characteristic electronic configuration have also been confirmed experimentally by mass spectrometry [39]. However, the stability descriptors shown in Fig. 2a and b characterize local stability within the two-dimensional Al–B compositional space rather than the absolute stability of an isolated composition. Thus, the larger Δ^2_{min} value of $Al_{13}B$ in Fig. 2a and the larger fragmentation energy of $Al_{12}B$ in Fig. 2b indicate that these clusters are even more stable with respect to neighboring compositions or competing fragmentation channels. This does not contradict the magic character of Al_{13} but rather indicates that neighboring Al-rich Al-B clusters can exhibit stronger local stabilization according to the specific criteria used here. The high stability of $Al_{12}B$ is also consistent with the available experimental mass-spectrometric data [40, 41]. Additionally, these clusters are highly resistant to decomposition as reflected in high values of the energy of fragmentation (Table S2, Sect. 1 of ESI). To further characterize the stability of the predicted clusters, we additionally analyzed the energetics of elementary composition-changing processes involving the addition or removal of a single atom (Fig. S3). This analysis complements the fragmentation criterion by identifying the energetically most accessible elementary change in cluster composition. Interestingly, throughout the entire composition range, the most favorable elementary process corresponds to the addition of a boron atom, whereas all single-atom removal processes remain energetically unfavorable.

We have used a third criterion, the HOMO-LUMO gap. Fig. 2c shows interpolated heatmaps of gaps for Al_nB_m nanoclusters. This gap is a key factor in determining the electronic properties of a cluster, such as its electronic polarisability (and, hence, reactivity). Nanoclusters with a wide HOMO-LUMO gap are typically less reactive and thus more easily survive interactions with other molecules. The largest HOMO–LUMO gaps are observed for the B_8 and AlB_8 clusters. This enhanced gap can be attributed to their high structural symmetry.

Prospects of Al-B nanoparticles in application of high energy density materials

We investigated the potential of Al_nB_m clusters as high-energy-density additives to organic fuels. We examined the combustion of any cluster leading to the most stable oxides of aluminum and boron. To better approximate real conditions, we consider the process at 300 K and ambient pressure, using Gibbs free energy.

We calculated the energy output obtained from burning a given cluster in an oxygen atmosphere, leading to the formation of stable products — Al_2O_3 and B_2O_3. We assume that each cluster reacts with O_2, producing Al_2O_3 and B_2O_3 with the corresponding stoichiometric coefficients:

$$Al_nB_m + \frac{3}{4}(n+m)O_2 -> \frac{1}{2}nAl_2O_3 + \frac{1}{2}mB_2O_3$$

The energetic output of the combustion reaction can be calculated as follows:

$$\Delta_c G(Al_nB_m) = -[\tfrac{1}{2}\mathrm{nG}(Al_2O_3) + \tfrac{1}{2}mG(B_2O_3)G(Al_nB_m) - \tfrac{3}{4}(n+m)G(O_2)] = -\Delta_r G(Al_nB_m)$$

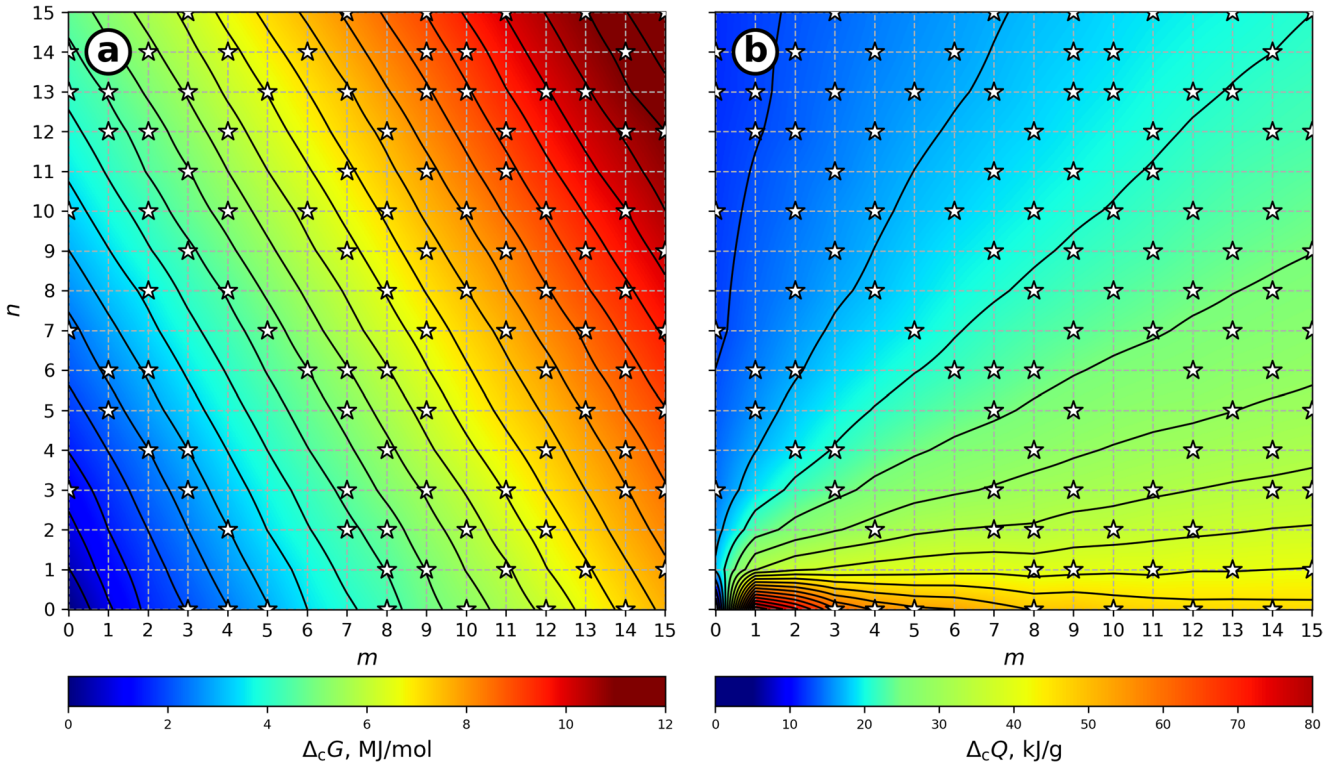

Fig. 3 Interpolated heatmaps of (**a**) Gibbs free energies of combustion, $\Delta_c G$ and (**b**) specific combustion energy, $\Delta_c Q$ for Al_nB_m nanoclusters. Stars highlight "magic" compositions of corresponding systems

where G is the Gibbs free energy of the corresponding compound.

The Gibbs free energies of combustion of Al_nB_m nanoclusters are presented as an interpolated two-dimensional heatmap (Fig. 3a). Here, $\Delta_c G(Al_nB_m)$ is taken with the opposite sign of the Gibbs free energy change, so that larger positive values correspond to more exothermic combustion. Figure 3b illustrates the specific combustion energy:

$$\Delta_c Q(\mathrm{Al}_n\mathrm{B}m) = \Delta_c G(\mathrm{Al}_n\mathrm{B}_m)/M(\mathrm{Al}_n\mathrm{B}_m)$$

where $M(Al_nB_m)$ is the molar mass of the Al_nB_m cluster. This quantity characterizes how intensely a given cluster "burns" per unit mass and allows direct comparison between clusters of different compositions. In boron-rich systems, actual oxidation can be limited by the formation of a B_2O_3 surface layer, whereas Al incorporation may facilitate oxidation by promoting aluminum borate formation and reducing diffusion-related limitations [42–44].

Pure boron clusters exhibit larger values of the Gibbs free energy of combustion ($\Delta_c G$) than aluminum clusters, which is in contrast to their bulk phases, in which aluminum combustion releases more energy: $\Delta_c G(Al_2O_3) = 1690.96$ kJ/mol, $\Delta_c G(B_2O_3) = 1288.12$ kJ/mol. This reverse behaviour at the nanoscale occurs due to dangling B-B bonds, making the surface energy of boron clusters very high.

Owing to the lower atomic masses of boron B-rich Al_nB_m nanoclusters exhibit the highest specific combustion energy, $\Delta_c Q$ (Fig. 3b). In addition, smaller clusters display enhanced values of $\Delta_c Q$, reflecting the increased fraction of undercoordinated surface atoms. However, the present analysis is limited to the thermodynamics of the initial clusters and final combustion products and does not include the full reaction pathways reaction or kinetic barriers.

Conclusions

In this work, we performed a systematic investigation of Al-B nanoclusters containing up to 32 atoms. Despite the isoelectronic nature of aluminum and boron, it is shown that their structural chemistry differs significantly both from each other and from that of mixed Al-B clusters. Pure aluminum clusters are prone to have delocalized covalent bonding (for large clusters and solids becoming metallic), whereas boron clusters tend to form multicenter directional covalent bonds. The structural motifs of Al-B clusters are determined by the interplay between directional B-B bonding and metallic interactions involving Al atoms. As a result, a structural evolution is observed from aluminum-rich globulal clusters to dense boron networks. Our analysis has uncovered numerous magic Al-B clusters, and we

find that fragmentation predominantly occurs through the loss of aluminum atoms, indicating stronger bonding within boron-rich frameworks. The clearest signature of stability is found for families of clusters satisfying the relation $n+m$ = 6, 12, 16, 18, 20, and 22, corresponding to closed electronic shells. However, additional stabilization is also observed for clusters with an odd number of electrons when they possess closed atomic shells due to high structural symmetry.

The combustion energetics reveal a pronounced nanoscale effect: boron-rich clusters exhibit higher Gibbs free energies of combustion and higher specific combustion energies than aluminum clusters, in contrast to the behavior observed in the bulk. This effect is associated with the low atomic mass of boron as well as the increased contribution of surface energy to the energetic characteristics of boron-containing clusters at the nanoscale. Accordingly, nanostructured covalently bonded materials, such as aluminum–boron clusters, may be of interest as high-energy additives to energetic mixtures due to the enhanced contribution of surface energy and their distinct structural chemistry compared to single-element clusters.

Supplementary Information The online version contains supplementary material available at https://doi.org/10.1007/s10876-026-03099-8.

Acknowledgements This work was supported by the Russian Science Foundation (grant #25-43-20043). The calculations were performed using a supercomputer at the Lebedev Physical Institute (LPI), the Oleg and Arkuda supercomputers at Skoltech, the Lobachevsky cluster at the University of Nizhny Novgorod, and the GOVORUN supercomputer at the Joint Institute for Nuclear Research (JINR).

Authors' contributions E.E.V. conceived the study, performed the structure prediction and quantum-chemical calculations, analyzed the data, and wrote the original draft of the manuscript. A.A.M. contributed to the methodology, data analysis, and manuscript editing. S.V.L. contributed to the conceptualization, methodology, analysis and interpretation of the results. A.P.M. contributed to the interpretation of the results and manuscript editing. A.R.O. supervised the project, contributed to the conceptualization and interpretation of the results, and critically revised the manuscript. All authors reviewed and approved the final manuscript.

Data availability No datasets were generated or analysed during the current study.

Declarations

Competing interests The authors declare no competing interests.

References

1. I.A.S. Ferrão, M.A.A. Mendes, A.S.O.H. Moita, A.R.R. Silva, The addition of particles to an alternative jet fuel, Fuels 3 (2022) 184–206. https://doi.org/10.3390/fuels3020012.
2. M. Jones, C.H. Li, A. Afjeh, G. Peterson, Experimental study of combustion characteristics of nanoscale metal and metal oxide additives in biofuel (ethanol), Nanoscale Res Lett 6 (2011) 246. https://doi.org/10.1186/1556-276X-6-246.
3. D. Sundaram, V. Yang, R.A. Yetter, Metal-based nanoenergetic materials: Synthesis, properties, and applications, Prog. Energy Combust. Sci. 61 (2017) 293–365. https://doi.org/10.1016/j.pecs.2017.02.002.
4. E.D. Anisimova, E.E. Vaneeva, V.S. Baturin, S.V. Lepeshkin, A.R. Oganov, Structural motifs and evolution of boron nanoclusters, J. Cluster Sci. 36 (2025). https://doi.org/10.1007/s10876-025-02815-0.
5. Y.-R. Luo, Comprehensive Handbook of Chemical Bond Energies, CRC Press, 2007. https://books.google.com/books/about/Comprehensive_Handbook_of_Chemical_Bond.html?hl=&id=kM3mwD4y_TAC.
6. A. Ulas, K.K. Kuo, C. Gotzmer, Ignition and combustion of boron particles in fluorine-containing environments, Combust. Flame 127 (2001) 1935–1957. https://doi.org/10.1016/s0010-2180(01)00299-1.
7. Q. Hu, Z. Wang, Z. Sun, Aluminum-based alloy fuels for solid propellants: Intrinsic properties, energy enhancement and combustion rate regulation, J. Alloys Compd. 1010 (2025) 177793. https://doi.org/10.1016/j.jallcom.2024.177793.
8. W. Pang, L.T. De Luca, X. Fan, O.G. Glotov, F. Zhao, Boron-based fuel-rich propellant: Properties, combustion, and technology aspects, CRC Press, 2019. https://doi.org/10.1201/9780429030680.
9. Makhov, M.N. Effect of aluminum and boron additives on the heat of explosion and acceleration ability of high explosives. *Russ. J. Phys. Chem. B* 9, 50–55 (2015). https://doi.org/10.1134/S199079311501008X
10. B.I. Lukhovitskii, A.S. Sharipov, Thermodynamic analysis of prospects for using aluminum- and boron-containing clusters in combined high-energy fuels, J. Eng. Phys. Thermophys. 91 (2018) 766–773. https://doi.org/10.1007/s10891-018-1799-7.
11. X.-J. Feng, Y.-H. Luo, Structure and stability of Al-doped boron clusters by the density-functional theory, J Phys Chem A 111 (2007) 2420–2425. https://doi.org/10.1021/jp0656429.
12. S. Jin, B. Chen, X. Kuang, C. Lu, W. Sun, X. Xia, G.L. Gutsev, Structural and electronic properties of medium-sized aluminum-doped boron clusters $AlB_n$and their anions, J. Phys. Chem. C Nanomater. Interfaces 123 (2019) 6276–6283. https://doi.org/10.1021/acs.jpcc.9b00291.
13. G. Kresse, J. Furthmüller, Efficient iterative schemes for ab initio total-energy calculations using a plane-wave basis set, Phys. Rev. B Condens. Matter 54 (1996) 11169–11186. https://doi.org/10.1103/physrevb.54.11169.
14. G. Kresse, J. Hafner, Ab initio molecular dynamics for liquid metals, Phys. Rev. B Condens. Matter 47 (1993) 558–561. https://doi.org/10.1103/physrevb.47.558.
15. P.E. Blöchl, Projector augmented-wave method, Phys. Rev. B Condens. Matter 50 (1994) 17953–17979. https://doi.org/10.1103/physrevb.50.17953.
16. J.P. Perdew, K. Burke, M. Ernzerhof, Generalized gradient approximation made simple, Phys. Rev. Lett. 77 (1996) 3865–3868. https://doi.org/10.1103/PhysRevLett.77.3865.
17. P.J. Stephens, F.J. Devlin, C.F. Chabalowski, M.J. Frisch, Ab initio calculation of vibrational absorption and circular dichroism spectra using density functional force fields, J. Phys. Chem. 98 (1994) 11623–11627. https://doi.org/10.1021/j100096a001.
18. D.V. Rybkovskiy, S.V. Lepeshkin, A.A. Mikhailova, V.S. Baturin, A.R. Oganov, Lithiation of phosphorus at the nanoscale: a computational study of LiP clusters, Nanoscale 16 (2024) 1197–1205. https://doi.org/10.1039/d3nr05166h.
19. E.E. Vaneeva, S.V. Lepeshkin, A.R. Oganov, Prediction and Rationalization of Abundant C-N-H Molecules in Different Environments, J. Phys. Chem. Lett. 14 (2023) 8367–8375. https://doi.org/10.1021/acs.jpclett.3c01753.

20. A.A. Mikhailova, S.V. Lepeshkin, V.S. Baturin, A.P. Maltsev, Y.A. Uspenskii, A.R. Oganov, Ultralow reaction barriers for CO oxidation in Cu-Au nanoclusters, Nanoscale 15 (2023) 13699–13707. https://doi.org/10.1039/d3nr02044d.
21. M. Fedyaeva, S. Lepeshkin, A.R. Oganov, Stability of sulfur molecules and insights into sulfur allotropy, Phys. Chem. Chem. Phys. 25 (2023) 9294–9299. https://doi.org/10.1039/d2cp05498a.
22. D.V. Rybkovskiy, S.V. Lepeshkin, V.S. Baturin, A.A. Mikhailova, A.R. Oganov, Phosphorus nanoclusters and insight into the formation of phosphorus allotropes, Nanoscale 15 (2023) 1338–1346. https://doi.org/10.1039/d2nr06523a.
23. S.V. Lepeshkin, V.S. Baturin, Y.A. Uspenskii, A.R. Oganov, Method for Simultaneous Prediction of Atomic Structure and Stability of Nanoclusters in a Wide Area of Compositions, J. Phys. Chem. Lett. 10 (2019) 102–106. https://doi.org/10.1021/acs.jpclett.8b03510.
24. S.V. Lepeshkin, V.S. Baturin, A.S. Naumova, A.R. Oganov, "Magic" Molecules and a New Look at Chemical Diversity of Hydrocarbons, J. Phys. Chem. Lett. 13 (2022) 7600–7606. https://doi.org/10.1021/acs.jpclett.2c02098.
25. E.E. Vaneeva, S.V. Lepeshkin, D.V. Rybkovskiy, A.R. Oganov, Exploring the diversity of molecular carbon oxides, and their potential as high energy density materials, Mater. Today Energy 49 (2025) 101821. https://doi.org/10.1016/j.mtener.2025.101821.
26. (n.d.). https://doi.org/10.1039/A807713D.
27. A. Aguado, J.M. López, Structures and stabilities of Al(n) (+), Al(n), and Al(n) (-) (n = 13–34) clusters, J Chem Phys 130 (2009) 064704. https://doi.org/10.1063/1.3075834.
28. X. Wu, L. Sai, S. Zhou, P. Zhou, M. Chen, M. Springborg, J. Zhao, Competition between tubular, planar and cage geometries: a complete picture of structural evolution of B (n = 31–50) clusters, Phys Chem Chem Phys 22 (2020) 12959–12966. https://doi.org/10.1039/d0cp01256d.
29. T.B. Tai, N.M. Tam, M.T. Nguyen, Structure of boron clusters revisited, Bn with n = 14–20, Chem. Phys. Lett. 530 (2012) 71–76. https://doi.org/10.1016/j.cplett.2012.01.039.
30. M. Atiş, C. Özdoğan, Z.B. Güvenç, Structure and energetic of B_n (n = 2–12) clusters: Electronic structure calculations, Int. J. Quantum Chem. 107 (2007) 729–744. https://doi.org/10.1002/qua.21171.
31. P.L. Rodríguez-Kessler, A. Vásquez-Espinal, A.R. Rodríguez-Domínguez, J.L. Cabellos-Quiroz, A. Muñoz-Castro, Structures of Ni-doped B (n = 1–13) clusters: A computational study, Inorganica Chim. Acta 568 (2024) 122062. https://doi.org/10.1016/j.ica.2024.122062.
32. P.L. Rodríguez-Kessler, A. Muñoz-Castro, A Zn-supported B wheel structure for the global minimum of the BZn cluster, Phys Chem Chem Phys 27 (2025) 3583–3587. https://doi.org/10.1039/d4cp04444d.
33. P.L. Rodríguez-Kessler, A. Muñoz-Castro, Structure search for B 7 Cr 2 clusters: Inverse sandwich structure for the global minimum, Polyhedron 273 (2025) 117486. https://doi.org/10.1016/j.poly.2025.117486.
34. P.L. Rodríguez-Kessler, A. Muñoz-Castro, AlB: an extension of the inverse sandwich B cluster featuring Lewis acid sites and planar aromaticity, Phys Chem Chem Phys 27 (2025) 12793–12800. https://doi.org/10.1039/d5cp01078k.
35. J.M. Guevara-Vela, J.L. Cabellos-Quiroz, S. Salazar-Colores, P.L. Rodríguez-Kessler, A. Muñoz-Castro, Structure search for B 7 Mn 2 clusters: Inverse sandwich geometry with a high-spin state, Comput. Theor. Chem. 1254 (2025) 115487. https://doi.org/10.1016/j.comptc.2025.115487.
36. J.M. Guevara-Vela, P.L. Rodríguez-Kessler, J.L. Cabellos-Quiroz, T. Rocha-Rinza, A. Vásquez-Espinal, A. Muñoz-Castro, Structure- and Size-Dependent Properties of BCu (=2–14) Clusters: DFT Calculations, J Phys Chem A 129 (2025) 4855–4860. https://doi.org/10.1021/acs.jpca.4c08443.
37. B.I. Loukhovitski, A.S. Sharipov, A.M. Starik, Quantum chemical study of small Al n B m clusters: Structure and physical properties, Chem. Phys. 493 (2017) 61–76. https://doi.org/10.1016/j.chemphys.2017.06.006.
38. A.J. Mannix, X.-F. Zhou, B. Kiraly, J.D. Wood, D. Alducin, B.D. Myers, X. Liu, B.L. Fisher, U. Santiago, J.R. Guest, M.J. Yacaman, A. Ponce, A.R. Oganov, M.C. Hersam, N.P. Guisinger, Synthesis of borophenes: Anisotropic, two-dimensional boron polymorphs, Science 350 (2015) 1513–1516. https://doi.org/10.1126/science.aad1080.
39. H. Wu, H. Zhang, L. Geng, Y. Jia, B. Huang, M. Yang, B. Yin, X. Lei, Z. Luo, Pure metal clusters with atomic precision for nanomanufacturing, Nanomanufacturing Metrol. 5 (2022) 230–239. https://doi.org/10.1007/s41871-022-00139-5.
40. A. Nakajima, T. Kishi, T. Sugioka, K. Kaya, Electronic and geometric structures of aluminum-boron negative cluster ions (Al B–), Chem. Phys. Lett. 187 (1991) 239–244. https://doi.org/10.1016/0009-2614(91)90419-a.
41. T. Inoue, M. Hatanaka, A. Nakajima, Oxidative Activation of Small Aluminum Nanoclusters with Boron Atom Substitution prior to Completing the Endohedral B@Al Superatom, J Am Chem Soc 145 (2023) 23088–23097. https://doi.org/10.1021/jacs.3c06191.
42. S. Adil, B.S. Murty, Effect of milling on the oxidation kinetics of Aluminium + Boron mixture and nanocrystalline Aluminium Boride (AlB12), Thermochim. Acta 678 (2019) 178306. https://doi.org/10.1016/j.tca.2019.178306.
43. M. Ma, G. Liu, Z. Qin, R. Zhang, Y. Ying, L. Xu, D. Liu, Effects of aluminum addition on flash ignition and combustion of boron nanoparticles, Combust. Flame 236 (2022) 111762. https://doi.org/10.1016/j.combustflame.2021.111762.
44. M.L. Whittaker, H.Y. Sohn, R.A. Cutler, Oxidation kinetics of aluminum diboride, J. Solid State Chem. 207 (2013) 163–169. https://doi.org/10.1016/j.jssc.2013.09.028.

Publisher's Note Springer Nature remains neutral with regard to jurisdictional claims in published maps and institutional affiliations.

Springer Nature or its licensor (e.g. a society or other partner) holds exclusive rights to this article under a publishing agreement with the author(s) or other rightsholder(s); author self-archiving of the accepted manuscript version of this article is solely governed by the terms of such publishing agreement and applicable law.